

Neural mass model parameter identification for MEG/EEG

Jan Kybic^a, Olivier Faugeras^b, Maureen Clerc^b, Théo Papadopoulo^b

^aCenter for Machine Perception, Faculty of Electrical Engineering, Czech Technical University, Prague, Czech Republic

^bOdyssée Laboratory – ENPC/ENS/INRIA, Sophia-Antipolis, France

ABSTRACT

Electroencephalography (EEG) and magnetoencephalography (MEG) have excellent time resolution. However, the poor spatial resolution and small number of sensors do not permit to reconstruct a general spatial activation pattern. Moreover, the low signal to noise ratio (SNR) makes accurate reconstruction of a time course also challenging. We therefore propose to use constrained reconstruction, modeling the relevant part of the brain using a neural mass model: There is a small number of zones that are considered as entities, neurons within a zone are assumed to be activated simultaneously. The location and spatial extend of the zones as well as the inter-zonal connection pattern can be determined from functional MRI (fMRI), diffusion tensor MRI (DTMRI), and other anatomical and brain mapping observation techniques. The observation model is linear, its deterministic part is known from EEG/MEG forward modeling, the statistics of the stochastic part can be estimated. The dynamics of the neural model is described by a moderate number of parameters that can be estimated from the recorded EEG/MEG data. We explicitly model the long-distance communication delays. Our parameters have physiological meaning and their plausible range is known. Since the problem is highly nonlinear, a quasi-Newton optimization method with random sampling and automatic success evaluation is used. The actual connection topology can be identified from several possibilities. The method was tested on synthetic data as well as on true MEG somatosensory-evoked field (SEF) data.

1. INTRODUCTION

There is currently no completely satisfactory approach to MEG/EEG reconstruction.^{1–4} Let us briefly review the options from the least to the most constrained ones: Completely unconstrained reconstruction is impossible because of small number of sensors as standard MEG or EEG machine has at most hundredths of sensors, while we normally want to reconstruct on a grid with $10^3 \sim 10^6$ elements. Classical minimum norm or beamformer type approaches^{5,6} provide non-focalized (blurry) estimates. We can force the reconstruction to provide focal estimates by suitable regularization,⁷ however there is no guarantee that the true activation is focal. Finally, classical dipole-localization techniques^{8,9} explain the observation by a single dipolar source, thus not making the full use of the available information.

We therefore propose to relax our original goal of reconstructing the brain activity from MEG/EEG only. We shall use our anatomical knowledge as well as other available imaging modalities, such as functional MRI (fMRI) or diffusion tensor MRI (DTMRI) to create a low-dimensional dynamic neural mass model.^{10–12} Such a model describes a brain activity using a low-dimensional vector representing activations in predefined zone. Moreover, the dynamics (time behavior) of the activations is restricted by a dynamical model. We can then use the high temporal resolution of MEG/EEG to identify the (mainly temporal) parameters of the model. Since we found that the physiology inspired standard neural mass models^{11,12} are too complicated to allow identification in realistic setting, in this version we use a simplified version.

email: kybic@fel.cvut.cz, tel: +420 2 2435 5721. This work was sponsored by the Czech-French bilateral project Barrande 2-06-3 and the Czech Ministry of Education under Project MSM6840770012.

2. METHODS

2.1. Observation model

It is generally accepted that a human cortex can be divided into functionally distinct areas called zones.^{13,14} The basic assumption is that there are no significant differences of activation intensity within each zone. Let us denote the number of zones relevant to the task at hand as N and the time course of their activity (corresponding to the post-synaptic potentials¹⁵) as $\mathbf{u}(t) = [u_1(t) \dots u_N(t)]^T$. The number of time points is T . The observed M dimensional MEG/EEG data are given by a linear equation

$$\mathbf{v}(t) = \mathbf{B}\mathbf{u}(t) + \mathbf{r}(t) \quad (1)$$

The $M \times N$ lead-field matrix \mathbf{B} is assumed to be known. It comes from the standard solution of the forward EEG/MEG problem^{16,17} and from the geometrical configuration of the zones. If the scaling of \mathbf{B} is not known, it can be estimated from the data by a simple least-squares procedure. There is an observation noise \mathbf{r} which is assumed to be zero-mean $E[\mathbf{r}] = \mathbf{0}$ and uncorrelated in time (for given sampling frequency); its spatial correlation matrix $\mathbf{P} = E_t[\mathbf{r}\mathbf{r}^T]$ can be estimated from the observations $\mathbf{v}(t)$ in intervals where no activation is present. Moreover we shall assume that \mathbf{r} is Gaussian.

Note that \mathbf{P} is symmetric positive definite and can be decomposed as $\mathbf{P} = \mathbf{P}^{1/2}\mathbf{P}^{1/2}$.

2.2. ML estimation

Ignoring the dynamics, we can calculate a maximum-likelihood (ML) estimate $\mathbf{u}^\dagger(t)$ for each time point independently:

$$\mathbf{u}^\dagger(t) = \arg \max_{\mathbf{u}} p(\mathbf{v}(t) | \mathbf{u})$$

which is equivalent to minimizing the quadratic error

$$\mathbf{u}^\dagger(t) = \arg \min_{\mathbf{u}} (\mathbf{v}(t) - \mathbf{B}\mathbf{u})^T \mathbf{P}^{-1} (\mathbf{v}(t) - \mathbf{B}\mathbf{u}) \quad (2)$$

thanks to our assumption of Gaussianity of \mathbf{r} . The solution is a standard pseudo-inverse

$$\mathbf{u}^\dagger(t) = \mathbf{Q}\mathbf{B}^T\mathbf{P}^{-1}\mathbf{v}(t) \quad \text{with} \quad \mathbf{Q} = (\mathbf{B}^T\mathbf{P}^{-1}\mathbf{B})^{-1} \quad (3)$$

2.3. Dynamic model

The zones are assumed to be connected by directional finite-delay transmission lines (see Figure 1 for an example). The first zone is activated by the stimulus, the activation is then transmitted through the network. Let us assume that the topology of the connections is known (we will address this limitation later) and that the connections form a directed acyclic graph.

There are good models for the dynamic behavior of a population of neurons (one zone), such as the popular model of Jansen and Rit.^{18,19} However, this model involves eight coupled differential equations with more than 10 \sim 11 parameters per zone. To this we need to add a delay and a connection strength parameters for each connection. Although encouraging results on parameter identification were presented in the literature¹¹ using the Bayesian model, in our experiments we found that the number of parameters was too large to be reliably estimated from the noisy EEG/MEG data. Especially troublesome was the first order approximation of the delay¹¹ which was not accurate enough for longer delays.

We have therefore decided to use a much simple second order linear convolutional model.¹⁰ The transmission line delays are denoted d_k , $k = 1 \dots K$, where K is the number of the graph edges (connections). The external stimulus is assumed to be a Dirac impulse at time $t = 0$. This impulse is transmitted through the network, so that a zone i receives a Dirac impulse as its input at time $\sum_{k \in C} d_k$, where C is a path from the input (stimulus) to the zone i . Since there might be several paths leading to zone i , the total input received by zone i is

$$s_i(t) = \sum_{C \in \mathcal{S}_i} \delta\left(t - \sum_{k \in C} d_k\right)$$

where \mathcal{S}_i is defined by the graph topology and contains a set of all paths C from the input (stimulus) to zone i , each path being represented as a set of delays encountered. For example, for the synthetic model in Figure 1, $\mathcal{S}_1 = \{\{1\}\}$, $\mathcal{S}_2 = \{\{1, 2\}\}$, $\mathcal{S}_3 = \{\{1, 2, 3\}\}$, and $\mathcal{S}_4 = \{\{1, 2, 4\}\}$.

The activity $u_i(t)$ of each zone is a convolution of its input $s_i(t)$ and an impulse response^{10, 11}

$$h_i(t) = h(t/\tau_i) \quad \text{with} \quad h(t) = \begin{cases} t e^{-t} & t > 0 \\ 0 & t \leq 0 \end{cases}$$

We have

$$u_i(t) = s_i(t) * h_i(t)$$

or equivalently

$$u_i(t) = \sum_{C \in \mathcal{S}_i} h_i\left(t - \sum_{k \in C} d_k\right)$$

Note that $h_i(t)$ is parameterized by the time delay τ_i . On the other hand, there is no parameter for the amplitude since this makes the estimation less robust and we consider that the amplitude effects have been taken care of in matrix \mathbf{B} .

The dynamic model can be described by a $K + N$ dimensional parameter vector $\theta = [\tau_1 \dots \tau_N \ d_1 \dots d_K]$. We assume the parameters to be independent. Since all parameters correspond to real physiological delays, we have a relatively good idea about the range of values a parameter can take. Specifically, the expected delays can be determined from known propagation speeds and distances between zones. We use a log-normal a priori probability density function (pdf)¹²

$$\log \theta_i \sim \mathcal{N}(\mu_i, \sigma_i) \quad (4)$$

2.4. Parameter estimation

We use a Bayesian approach to estimate the unknown parameters $\theta = [\tau_1 \dots \tau_N \ d_1 \dots d_K]$ by maximizing the likelihood $p(\theta \mid \{\mathbf{v}(t)\}_t)$ where $\{\mathbf{v}(t)\}_t$ is the set of all observations $\mathbf{v}(t)$. By Bayes rule this is equivalent to maximizing the probability $p(\{\mathbf{v}(t)\}_t \mid \theta) p(\theta)$ which thanks to the i.i.d noise assumption can be decomposed as

$$p(\theta \mid \{\mathbf{v}(t)\}_t) = \frac{p(\theta) \prod_t p(\mathbf{v}(t) \mid \theta)}{p(\{\mathbf{v}(t)\}_t)} \quad (5)$$

This is in turn equivalent to minimizing the following cost function

$$J'(\theta) = \underbrace{\frac{1}{2} \sum_t (\mathbf{v}(t) - \mathbf{B}\mathbf{u}(\theta; t))^T \mathbf{P}^{-1} (\mathbf{v}(t) - \mathbf{B}\mathbf{u}(\theta; t))}_{J'_1} + \underbrace{\sum_{i=1}^{N+K} \frac{(\log \theta_i - \mu_i)^2}{2\sigma_i^2}}_{J_2} \quad (6)$$

Note that $\mathbf{u}(\theta; t)$ is a function of θ . The first part (J'_1) of the equation (6) above is the same as (2) (for each t). It is therefore not surprising that the first part reaches its minimum at $\mathbf{u}^\dagger(t)$ (from (3)). Its quadratic cost matrix is $\mathbf{B}^T \mathbf{P}^{-1} \mathbf{B} = \mathbf{Q}^{-1}$. Hence, minimizing $J'(\theta)$ is equivalent to minimizing the following $J(\theta)$.

$$J(\theta) = \underbrace{\frac{1}{2} \sum_t (\mathbf{u}^\dagger(t) - \mathbf{u}(\theta; t))^T \mathbf{Q}^{-1} (\mathbf{u}^\dagger(t) - \mathbf{u}(\theta; t))}_{J_1} + \underbrace{\sum_{i=1}^{N+K} \frac{(\log \theta_i - \mu_i)^2}{2\sigma_i^2}}_{J_2} \quad (7)$$

The advantage of minimizing J instead of J' is the reduction of dimensionality, as the dimension of \mathbf{u} is the number of zones N , which is much smaller than the number of sensors M . Note that the difference $J - J'$ is constant and does not depend on θ :

$$\begin{aligned} J(\theta) - J'(\theta) &= \frac{1}{2} \sum_t \mathbf{u}^\dagger(t)^T \mathbf{Q}^{-1} \mathbf{u}^\dagger(t) - \mathbf{v}^T(t) \mathbf{P}^{-1} \mathbf{v}(t) \\ &= \frac{1}{2} \sum_t \mathbf{v}^T(t) \left(\mathbf{P}^{-1} \mathbf{B} (\mathbf{B}^T \mathbf{P}^{-1} \mathbf{B})^{-1} \mathbf{B}^T \mathbf{P}^{-1} - \mathbf{P}^{-1} \right) \mathbf{v}(t) \end{aligned} \quad (8)$$

$$(9)$$

We minimize $J(\theta)$ using a quasi-Newton BFGS-like²⁰ algorithm. It converges quickly provided that a good starting point is given. However, our optimization problem is quite non-linear and it is not obvious to find a good starting point. We therefore randomly generate starting points θ_0 by sampling from the a priori parameter distribution (4). An optimization result is only accepted if $J(\theta)$ is smaller than some predetermined threshold α (see below). As soon as a predetermined number (e.g. 10) of acceptable results is assembled, the best one is taken to be the final result.

To determine a suitable threshold α , we need to determine the probability distribution of J at optimum θ . Let us start by the value of J_1 . By substitution from (1) and from the definition of \mathbf{P} , we find that $\mathbf{u}^\dagger(\theta; t) - \mathbf{u}(t)$ is normal and

$$\mathbb{E}[(\mathbf{u}^\dagger(\theta; t) - \mathbf{u}(t))(\mathbf{u}^\dagger(\theta; t) - \mathbf{u}(t))^T] = \mathbf{Q}$$

and through simple algebraic manipulation assuming the decomposability of $\mathbf{Q} = \mathbf{Q}^{1/2} \mathbf{Q}^{1/2}$ we have

$$\mathbb{E}[\mathbf{Q}^{-1/2}(\mathbf{u}^\dagger(\theta; t) - \mathbf{u}(t))(\mathbf{u}^\dagger(\theta; t) - \mathbf{u}(t))^T \mathbf{Q}^{-1/2}] = \mathbf{I}$$

Consequently $2J_1$ is a sum of TN squared i.i.d Gaussian normal random variables $\mathcal{N}(0, 1)$. In other words, $2J_1$ is distributed as χ_{TN}^2 . Similarly, from (4) and (7) we see that the second part, $2J_2$, has a χ_{N+K}^2 distribution. This yields

$$2J \sim \chi_{NT+N+K}^2$$

The threshold α can be then calculated easily given an acceptable probability ε of rejecting a valid solution using the inverse cumulative distribution function for the χ^2 distribution

$$P(\chi_{NT+N+K}^2 > \alpha) = \varepsilon$$

2.5. Topology estimation

If the topology of the zone connections is unknown, we can run the above minimization for each admissible graph. A connection graph is admissible if it contains no cycles and there is a path from the input to all zones. This is feasible for small number of zones. Note, though that several configuration might lead to the same activation pattern.

In practice we test several alternative models choosing the one with the smallest criterion value J .

3. RESULTS

3.1. Synthetic data

Figure 1 shows a simple model (top left) with 4 zones and 4 connections ($N = 4$, $K = 4$). We have generated $M = 100$ channel observations for $T = 501$ time points by spatial smoothing and adding Gaussian i.i.d. noise with relative amplitude 1% (top right) to the model output. The a priori distribution (4) was quite flat, with $\sigma = 2$ for the zone time constants τ and $\sigma = 3$ for the delays, the a priori means μ_i were 20 ms and 50 ms for the zones and delays, respectively.

We see that the ML estimate (3) is quite noisy while our constrained reconstruction yields almost perfect results, the recovered activity coinciding almost exactly with the true values. The topology was assumed known.

3.2. Real data

We have run our algorithm on MEG somatosensory evoked field data. The data were aligned and temporally averaged with respect to the stimulus onset. After a PCA analysis, we have also subtracted the principal component occurring immediately after the stimulus since we assume it corresponds to an unwanted interaction between the stimulation and sensor circuits. The resulting signals are shown in Figure 2.

From the a priori physiological knowledge, we assume a 3 zone model¹¹ consisting of contralateral zones cSI, cSII, and a zone iSII in the other hemisphere (Figure 4). Since neither the geometrical model nor the location of these zones for this particular anatomy was known, we had to use an alternative approach to estimate the lead field matrix B . We have identified three temporal maxima of the MEG signals at times 34 ms, 70 ms, and 96 ms that we assume correspond to the maximum activation of the three relevant zones. The three columns of matrix B have been composed of the measured MEG signals at these three times. Figure 3 shows the surface field at these moments.

We see that the ML reconstruction is quite noisy (Figure 4). Our constrained reconstruction looks plausible and explains the data well.

4. DISCUSSION

A related approach was described by Kiebel et al.,¹¹ who use a neural mass model of Jansen and Rit,¹⁹ which is too complex for this purpose, consisting of 8 coupled differential equations with tens of parameters per zone. Consequently, it is very difficult to estimate the parameters reliably from real data. In our approach, simpler and more easily identifiable model is used. Nevertheless, we take into account transport delays exactly, as we assume them to be very relevant for this application, while Kiebel et al. use a first-order approximation¹⁹ which is only appropriate for very small delays.

5. CONCLUSIONS

We have presented a practical method for identification of parameters for neural mass models from EEG/MEG data. The approach can take advantage of available geometrical and connection information from fMRI and DTMRI, using EEG/MEG to identify the time-related parameters. Although the models are simple, they seem to yield plausible reconstructions and permit evaluation of the delay parameters. In the future, we hope to make our models more realistic, while maintaining their identifiability from the data.

REFERENCES

1. J. Phillips, R. Leahy, J. Mosher, and B. Timsari, “Imaging neural activity using MEG and EEG,” *IEEE Engineering in Medicine and Biology Magazine* **16**(3), pp. 34–42, 1997.
2. J. Sarvas, “Basic mathematical and electromagnetic concepts of the biomagnetic inverse problem,” *Phys. Med. Biol.* **32**(1), pp. 11–22, 1987.
3. M. Hämäläinen, R. Hari, R. J. Ilmoniemi, J. Knuutila, and O. V. Lounasmaa, “Magnetoencephalography— theory, instrumentation, and applications to noninvasive studies of the working human brain,” *Reviews of Modern Physics* **65**, pp. 413–497, Apr. 1993.
4. S. Baillet, J. C. Mosher, and R. M. Leahy, “Electromagnetic brain mapping,” *IEEE Signal Processing Magazine* (18), pp. 14–30, 2001.
5. R. Pascual-Marqui, “Review of methods for solving the EEG inverse problem,” *International Journal of Bioelectromagnetism* **1**(1), pp. 75–86, 1999.
6. D. P. Schwartz, A. K. Liu, G. Bonmassar, and J. Belliveau, “Comparison of the linear estimation and spatio-temporal fit inverse approaches,” *International Journal of Bioelectromagnetism* **3**(1), 2001.
7. G. Adde, M. Clerc, R. Keriven, and J. Kybic, “Regularization for the inverse EEG/MEG problem using the symmetric boundary element method,” in *Proceedings of the 4th International Symposium on Noninvasive Functional Source Imaging (NFSI)*, V. Pizzella and G. L. Romani, eds., pp. 287–289, Organ of the German Society for Biomedical Engineering in VDE, (Berlin, Germany), September 2003.

8. J. C. Mosher, P. S. Lewis, and R. M. Leahy, "Multiple dipole modeling and localization from spatio-temporal MEG data," *IEEE Transactions on Biomedical Engineering* **39**(6), pp. 541–553, 1992.
9. A. M. Murro, J. R. Smith, D. W. King, and Y. D. Park, "Precision of dipole localization in a spherical volume conductor: a comparison of referential eeg, magnetoencephalography and scalp current density methods.," *Brain Topography* **8**(2), pp. 119–125, 1995.
10. V. K. Jirsa, "Connectivity and dynamics of neural information processing," *Neuroinformatics* **2**, pp. 1–22, 2004.
11. S. J. Kiebel, O. David, and K. J. Friston, "Dynamic causal modelling of evoked responses in EEG/MEG with lead field parameterization," *NeuroImage*, 2006. in press.
12. O. David, S. J. Kiebel, L. M. Harrison, J. Mattout, J. Kilner, and K. J. Friston, "Dynamic causal modeling of evoked responses in EEG and MEG," *NeuroImage* (30), pp. 1255–1272, 2006.
13. A. Anwender, M. Tittgemeyer, D. von Cramon, A. Friederici, and T. R. Knosche, "Connectivity-based parcellation of Broca's area," *Cerebral Cortex*, May 2006. in print.
14. J. Bullier, "Integrated model of visual processing," *Brain Research Reviews* (36), pp. 96–107, 2001.
15. B. Horwitz, K. J. Friston, and J. G. Taylor, "Neural modeling and functional brain imaging: an overview," *Neural Networks (Special Issue)* (13), pp. 829–846, 2000.
16. J. Kybic, M. Clerc, T. Abboud, O. Faugeras, R. Keriven, and T. Papadopoulos, "A common formalism for the integral formulations of the forward EEG problem," *IEEE Transactions on Medical Imaging* **24**, pp. 12–28, Jan. 2005.
17. J. C. Mosher, R. B. Leahy, and P. S. Lewis, "EEG and MEG: Forward solutions for inverse methods," *IEEE Transactions on Biomedical Engineering* **46**, pp. 245–259, Mar. 1999.
18. B. H. Jansen and V. G. Rit, "Electroencephalogram and visual evoked potential generation in a mathematical model of coupled cortical columns," *Biol. Cybern.* (73), pp. 357–366, 1995.
19. O. David, L. Harrison, and K. J. Friston, "Modelling event-related responses in the brain," *NeuroImage* (25), pp. 756–770, 2005.
20. W. H. Press, S. A. Teukolsky, W. T. Vetterling, and B. P. Flannery, *Numerical Recipes in C*, Cambridge University Press, second ed., 1992.

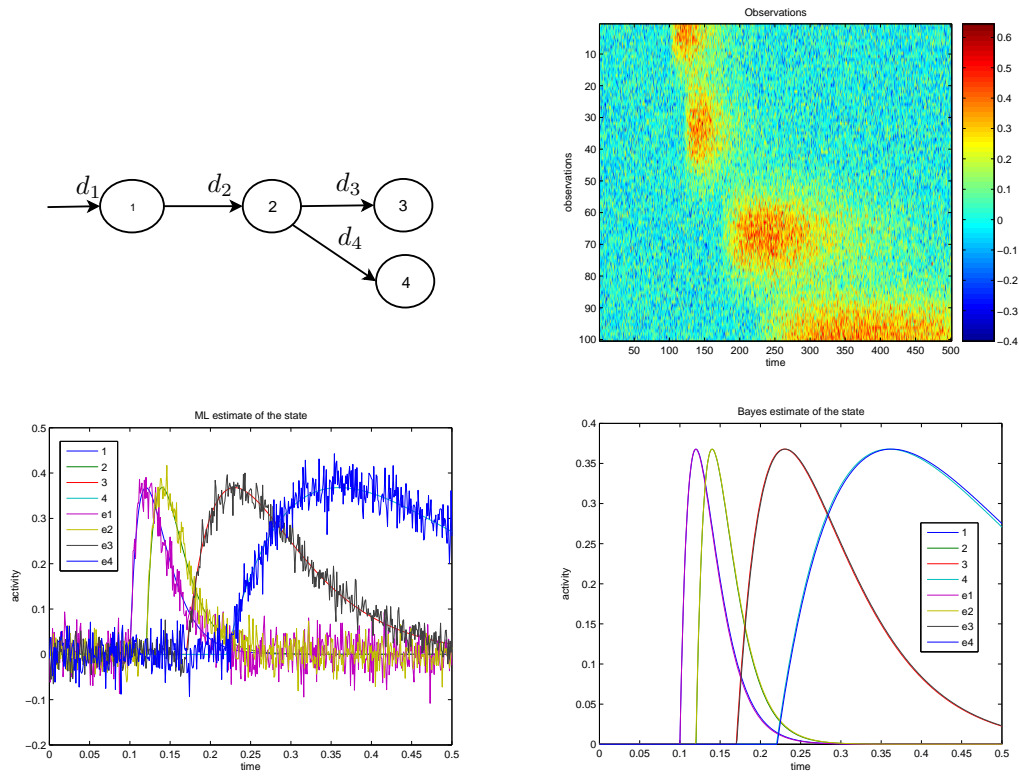


Figure 1. The synthetic case. Connection graph (top left), observation (top right), ML estimation (bottom left), and our results (bottom right)

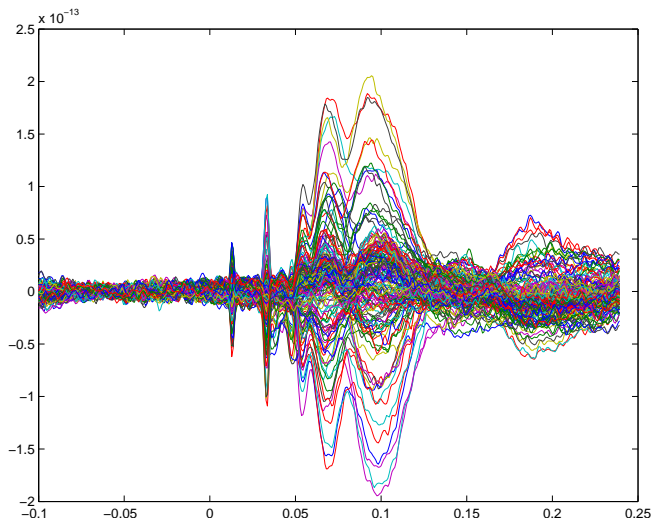


Figure 2. Averaged and cleaned MEG SEP signals.

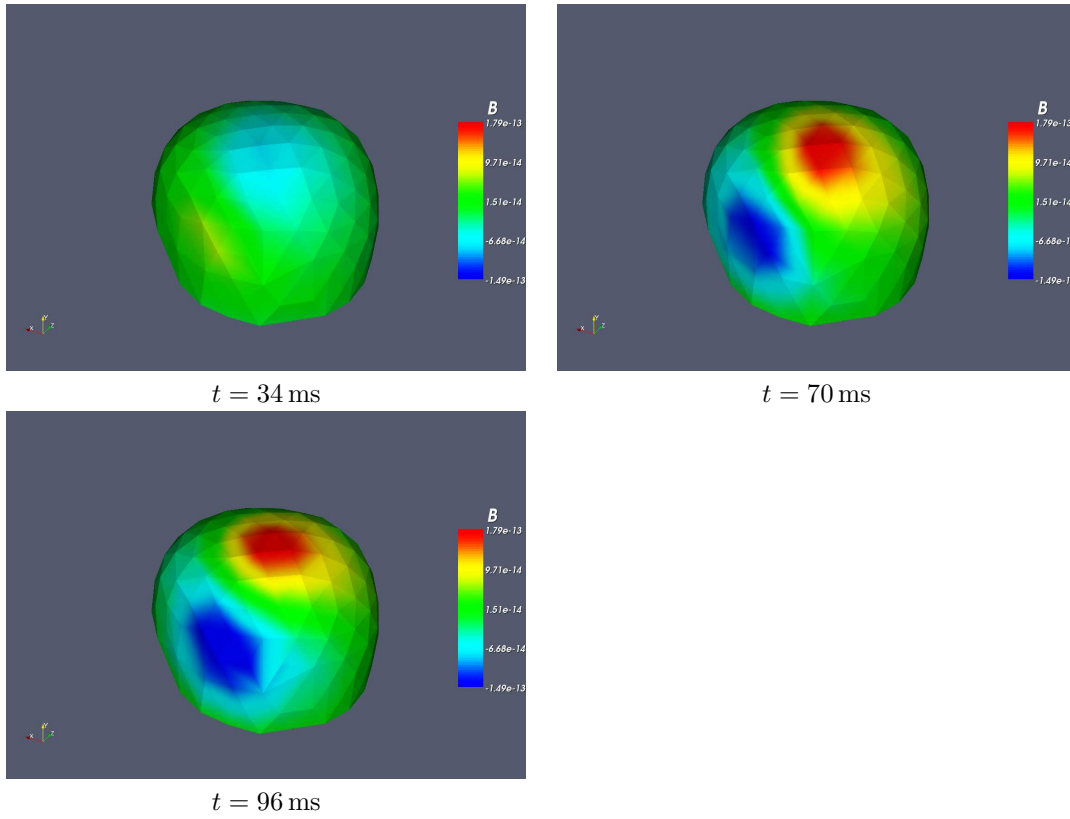


Figure 3. Surface MEG field at different times after the stimulus.

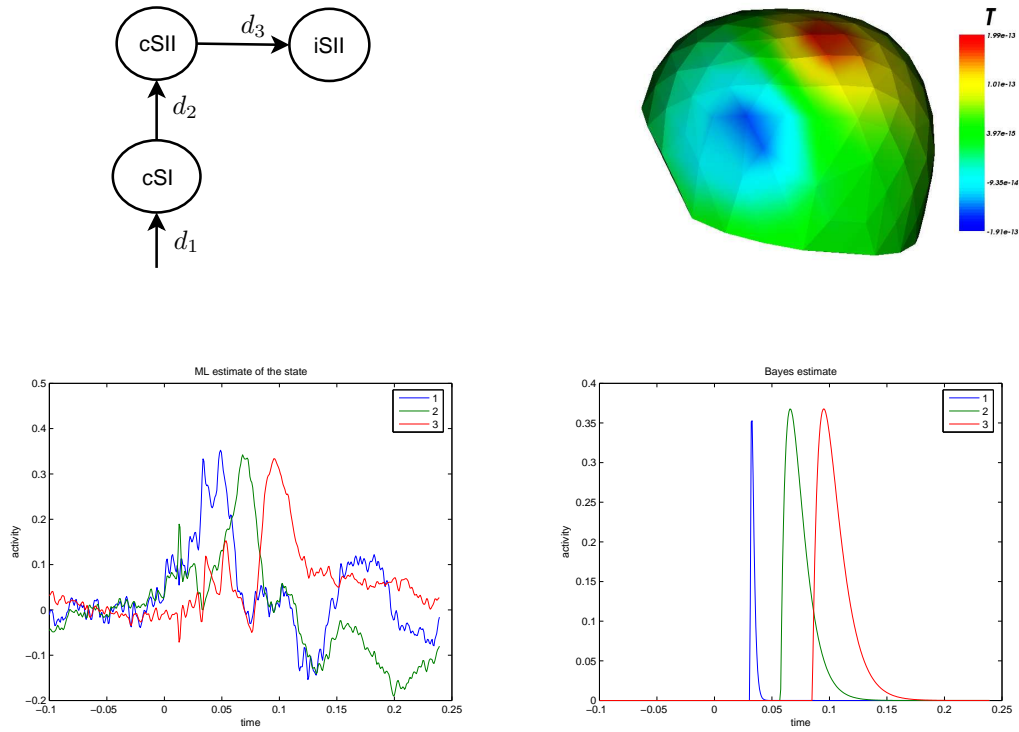


Figure 4. Real SEP data. Connection graph (top left), MEG at $t = 69$ ms (top right), ML estimation (bottom left), and our results (bottom right)